Int J Adv Manuf Technol (2016) 84:1705–1715
DOI 10.1007/s00170-015-7985-2

ORIGINAL ARTICLE

Specific cutting force and cutting condition interaction modeling for round insert face milling operation

Hamid Ghorbani[1] · **Behnam Moetakef-Imani**[1]

Received: 13 June 2015 / Accepted: 14 October 2015 / Published online: 24 October 2015

Abstract Face milling by round insert is currently one of the most common processes for roughing, semi-finishing, and finishing machining operations. Proper estimation and analysis of the round insert cutting forces play an important role in the process optimization. This paper presents a new method for identifying specific cutting force coefficients (SCFCs) for full immersion face milling with round inserts. At the first step, an inverse method is proposed to solve the mechanistic force model equations by non-dominated sorting genetic algorithm II (NSGA-II) which is one of the powerful multi-objective optimization methods. In addition, the artificial neural network (ANN) models are developed to predict the SCFCs in non-experimented conditions. Mean absolute percentage error values for the proposed ANN are between 1.7 and 10.1 % for training and testing which are satisfactory. In order to evaluate the efficiency of NSGA-II and ANN models, extensive experimental cutting force results are compared with those obtained with the proposed algorithm. The good accordance in the entire time of cutting edge engagement shows the validity of the developed methodology. Moreover, the interactions of cutting parameters, i.e., cutting speed, feed per tooth, and depth of cut (DOC) on variations of tangential and radial shearing coefficients (k_{tc}, k_{rc}) of specific cutting force are thoroughly investigated. The results show that in addition to cutting conditions, the cutting edge geometry of round insert has a significant influence on k_{tc} and k_{rc} variations.

Keywords Specific cutting force coefficients (SCFCs) · Face milling · Round insert · Multi-objective optimization method · Non-dominated sorting genetic algorithm II (NSGA-II) · Artificial neural network (ANN)

1 Introduction

Reaching to high material removal rate and relatively smooth surface finish are the most important aims in machining of metallic parts. Face milling by multiple-tooth cutter is a widely used machining process in mass production of functional surface [1]. Knowledge of cutting forces plays an important role in prediction of power, torque, and machine tool vibrations during milling operations [2, 3]. Many studies were performed to calculate and predict the instantaneous milling cutting forces. A machining literature review shows that three basic approaches are as follows: analytical, numerical, and mechanistic modeling. Analytical models focus on mathematical relationships between cutting forces and various physical parameters such as friction, cutting edge rake angle, and seizure [4]. The numerical or finite element methods studies the tool tip contact zone, distribution of temperature, and stress on the tool tip and in addition displacement of tool or workpiece [5, 6]. In the third approach, mechanistic modeling of the cutting forces is followed. Mechanistic modeling is not only based on metal cutting mechanics but also dependent on experimental tests data. In this approach, a combination of analytical and experimental modeling procedures are used [7]. In mechanistic modeling, the cutting force dependence on the chip load, cutting conditions, and workpiece tool materials are derived [2].

In the mechanistic method, usually cutting forces are expressed as a sum of two separate terms, i.e., shearing forces and edge forces [8–10].

✉ Behnam Moetakef-Imani
imani@um.ac.ir

[1] Department of Mechanical Engineering, Engineering Faculty, Ferdowsi University of Mashhad, Mashhad, Iran

Many studies have been done to empirically determine the shear and edge cutting force coefficients. Often, these coefficients were obtained based on mean force measurements per revolution for desired immersions [2, 8, 11]. In addition, in some recent research work, specific cutting force coefficients (SCFCs) were obtained from orthogonal cutting test data [12]. In some cases, the SCFCs of mechanistic approach are determined using the inverse way [13, 14]. The SCFCs are obtained by equating the analytical expressions of cutting forces to their average of measured cutting forces for a series experiments. Experimental works are usually conducted for slot milling at different feed rates in constant radial and axial immersions [13–16].

Round inserts with strong cutting edge and superior geometrical features spreads the force and heat distributions more evenly. Therefore, cutting edge wear is reduced and consequently fair surface finish is obtained [17, 18]. Due to complex geometry of the round insert, the pronounced effects of cutting edge entrance, and exit zones on the cutting forces, the average of cutting forces during engagement will introduce modeling errors. Thus, improved models incorporate the instantaneous cutting forces during engagement in order to determine the SCFCs [13].

Current work presents a new method for calculating the SCFCs using an inversed mechanistic model by equating the instantaneous and measured cutting forces during the cutting edge and workpiece engagement. The problem can be considered as a multi-objective problem where objective functions are the sum of squared errors between the simulated and measured instantaneous cutting forces in X, Y, and Z directions. Variables are SCFCs which should be determined such that the objective functions are minimized. In this research, the non-dominated sorting genetic algorithm II (NSGA-II) is used in order to find the optimal solution of multi-objective optimization problem. Moreover, the artificial neural network (ANN) models are developed to predict the SCFCs in non-experimented conditions. Mean absolute percentage error (MAPE) values of training and test data for the proposed ANNs are used to assess the computed models.

Henceforth, this paper is organized as follows: Sect. 2 introduces the chip geometry for the round insert of face milling. The mechanistic modeling approach for instantaneous cutting force modeling is proposed in Sect. 3. The next section presents a new method for obtaining the SCFCs using multi-objective optimization method. Section 5 demonstrates an experimental set up for validating proposed multi-objective optimization method. The proposed ANN topology which efficiently predicts the SCFCs in non-experimented cutting conditions is explained in the next section. The results of cutting force simulations are compared with measured values in Sect. 7. The cutting parameters interaction on tangential and radial shearing cutting coefficients (k_{tc}, k_{rc}) are also discussed in this section. Finally, the last section summarizes and concludes the current research work.

2 Instantaneous chip geometry for round insert

In face milling process, the instantaneous chip thickness varies continuously during engagement. Assuming a circular trajectory for the cutting edge, the following equation can express the variation of instantaneous chip thickness (see Fig. 1) [11]:

$$C_l(\theta_k(\phi)) = f_t.\sin(\theta_k(\phi)) \tag{1}$$

where $C_l(\theta_k)$ is chip thickness, f_t is feed per tooth, and $\theta_k(\phi)$ is angular position of kth insert in the ϕ cutter rotation angle. As seen in Fig. 2, the chip thickness distribution along the cutting edge of a round insert is not constant and varies along the edge. Minimum chip thickness is located at the zero axial DOC, and the maximum chip thickness occurs at the a_p axial DOC. The chip section is subdivided into differential discrete elemental areas dA, which is marked with crosshatch in Fig. 2. The thickness [2] and width of the element are shown by h and db, respectively, and specified by the following:

$$\begin{aligned} h &= C(\theta_k(\phi))\cdot\sin(\psi) \\ d\ b &= r \cdot d\ \psi \\ d\ A &= h \cdot d\ b \end{aligned} \tag{2}$$

where r is the insert radius and $d\psi$ is the angular increment of cutting edge, which is set to 0.1^0.

3 Mechanistic modeling of cutting forces

According to Sect. 2, the width and thickness of each element are computed and the elemental cutting forces are then determined. In the mechanistic model proposed by Budak et al. [12], cutting forces of each element in the tangential (dF_T),

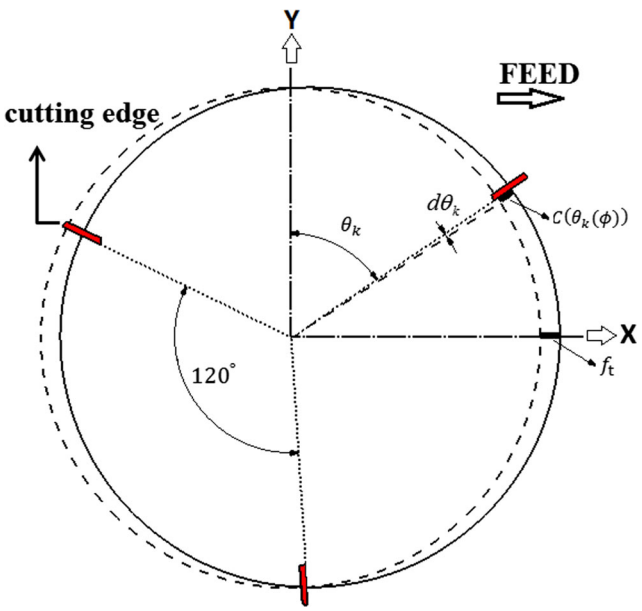

Fig. 1 Cutter tool path and instantaneous chip thickness of kth insert at θ_k

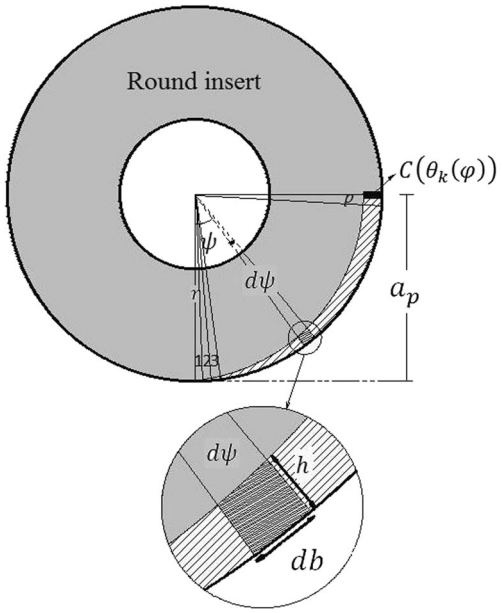

Fig. 2 Chip thickness variation along the round cutting edge

radial (dF_R), and axial (dF_A) directions, which are shown in Fig. 3, are calculated by the following relationships [12]:

$$\begin{aligned} dF_T &= K_{tc}dA + K_{te}db = (K_{tc}h + K_{te})\cdot db \\ dF_R &= K_{rc}dA + K_{re}db = (K_{rc}h + K_{re})\cdot db \\ dF_A &= K_{ac}dA + K_{ae}db = (K_{ac}h + K_{ae})\cdot db \end{aligned} \tag{3}$$

The equations include two terms. The first term consists of shearing coefficients (K_{tc}, K_{rc}, K_{ac}) that are multiplied by undeformed chip section (dA), and the second term consists of edge coefficients (K_{te}, K_{re}, K_{ae}) that are multiplied by width of cut (db). The shearing coefficients represent the influence of shearing at the shear zone and friction at the rake face on the cutting forces. Also, the edge coefficients represent the influence of rubbing or ploughing at the cutting edge on the cutting forces [12, 13]. The X (feed), Y (normal), and Z (axial) direction of cutting forces are obtained by transforming the tangential, radial, and axial cutting forces of each element which are shown in Fig. 3 and can be written as follows [12]:

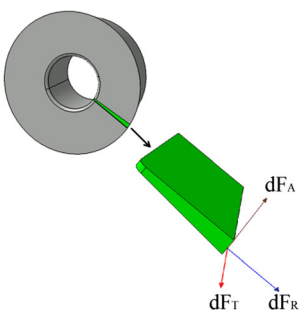

Fig. 3 Force components of a discrete element on the round cutting edge

$$\begin{bmatrix} dF_X \\ dF_Y \\ dF_Z \end{bmatrix} = \begin{bmatrix} -\cos(\phi) & -\sin(\phi)\sin(\psi) & -\sin(\phi)\cos(\psi) \\ \sin(\phi) & -\cos(\phi)\sin(\psi) & -\cos(\phi)\cos(\psi) \\ 0 & \cos(\psi) & -\sin(\psi) \end{bmatrix} \begin{bmatrix} dF_T \\ dF_R \\ dF_A \end{bmatrix} \tag{4}$$

The total cutting forces in feed (F_X), normal (F_Y), and axial (F_Z) direction can be achieved through integrating forces of each cutting edge [12]:

$$\begin{bmatrix} F_X \\ F_Y \\ F_Z \end{bmatrix} = \sum_{1}^{z}\sum_{1}^{p} \begin{bmatrix} dF_X \\ dF_Y \\ dF_Z \end{bmatrix} \tag{5}$$

where z is the number of cutter edges or inserts and P is the total number of differential elements on the cutting edge and given by

$$P = \frac{\cos^{-1}\left(\frac{r-a_p}{r}\right)}{d\psi} \tag{6}$$

4 A new method for obtaining SCFCs of mechanistic model

The proposed method for calculating the SCFCs is based on using an optimization method. By use of this method, the total engagement time can be an effective influence in the inverse solution of instantaneous cutting forces mechanistic equation. Substituting relations (3) and (4) in Eq. (5), the force at any discrete time, t, can be written as follows:

$$\begin{bmatrix} F_X \\ F_Y \\ F_Z \end{bmatrix}_t = G(h,b,t,\phi,\psi) \begin{bmatrix} K_{tc} \\ K_{te} \\ K_{rc} \\ K_{re} \\ K_{ac} \\ K_{ae} \end{bmatrix} \tag{7}$$

Equating the simulated and experimental forces in n discrete times, t, the equation systems are as follows:

$$\begin{bmatrix} \begin{bmatrix} F_X \\ F_Y \\ F_Z \end{bmatrix}_{t1} \\ \vdots \\ \begin{bmatrix} F_X \\ F_Y \\ F_Z \end{bmatrix}_{tn} \end{bmatrix}^{exp} = \begin{bmatrix} G(h,b,t,\phi,\psi)_{t1} \\ \vdots \\ G(h,b,t,\phi,\psi)_{tn} \end{bmatrix} \begin{bmatrix} K_{tc} \\ K_{te} \\ K_{rc} \\ K_{re} \\ K_{ac} \\ K_{ae} \end{bmatrix} \tag{8}$$

where n is the size of sample data and depends on the sampling frequency during the experimental tests. After measuring the experimental cutting force and calculating the instantaneous chip's cross-sectional area of each discrete time, t, SCFCs are the only unknown parameters of Eq. 8. In this research, a new method has been suggested to determine SCFCs using multi-objective optimization method. In this

method, the NSGA-II is used for solving the very large system of equation result of Eq. 8.

4.1 Multi-objective optimization method

Multi-objective optimization is one of the most widely used methods in the optimization problems [19]. In a single-objective optimization problem, there is usually a unique optimal solution. But, in multi-objective optimization problems, the objective functions may be conflicting with each other. A general method to solve multi-objective problems is transforming the multi-objective into one combined objective function. In this approach, it is proposed to multiply each objective function by a proper weighting factor. All contributors are integrated into a single objective function. However, selecting the appropriate weighting factors for the objective functions is a challenging task [19]. Therefore, it can be difficult to find precise and accurate solution for all objectives simultaneously. Another approach to solve multi-objective problems is to determine Pareto optimal solutions. Pareto optimal solutions are a set of results which each of them is not dominated by any other [19, 20]. The former method was used in this work. Given the cutting force in x, y, and z coordinates, the force system of equation (Eq. 8) is obtained as a three objective optimization problem. The objective functions are the sum of squared errors between empirical and simulated instantaneous cutting forces for each direction which can be expressed by the following:

$$E_i = \sum_n \| y_i - f_i(K_{tc}, K_{te}, K_{rc}, K_{re}, K_{ac}, K_{ae}, t) \|^2 \quad (9)$$

where y_i is the X, Y, and Z instantaneous experimental cutting forces and f_i represents the simulated cutting forces.

4.2 Multi-objective optimization using genetic algorithm

During the past decades, population-based optimization algorithms such as genetic algorithm are commonly used in multi-objective optimization problems such as machining process [21–23]. Genetic algorithm can achieve reasonable answers to create non-dominated solutions of the Pareto front with respect to conflict objectives [19]. NSGA-II is one of the most efficient multi-objective optimization algorithms [24]. In this study, NSGA-II is used to achieve the optimal solutions of three-objective optimization problem of the cutting force mechanistic model. The NSGA-II used includes the following major steps:

Step 1: Creating a set of search points called the initial population which is randomly determined (*initialization*)

Step 2: Evaluating the fitness function of each chromosome of the population (*fitness evaluation)* and sorting based on non-domination criteria.

Step 3: Producing the new generations using three operators: selection (making then mating pool based on tournament method), crossover, and mutation. The new generation has higher fitness than the previous generation which means that from current generation to the next one the fitness of the population improves.

Step 4: The search would stop if the maximum generation is considered or the stopping and convergence criteria is satisfied.

The values of parameters used in the NSGA-II are shown in Table 1.

5 Experimental work

The experiments carried out on a vertical CNC machining center with a Siemens 802D control system. The workpiece material was aluminum 7075-T6 which is usually used in the aerospace industry. Experimental tests were performed by a 42-mm diameter face mill cutter with three round inserts under dry cutting condition. The round insert, which has a radius of 6 mm, was a tungsten carbide TTI–15 produced by WIDIA. The axial and radial rake angles of cutter were 7.74° and 2.3°, respectively. Cutting force components were measured using a three-axis Kistler 9255B table dynamometer. Cutting conditions for milling tests are shown in Table 2.

A full factorial design of experiment is introduced to effectively investigate the interaction of independent variables. In this regard, 125 experiments were conducted and the X, Y, and Z forces were measured accordingly.

In order to increase the accuracy of results, each experiment has been repeated three times. The experimental setup used for performing the experiments is depicted in Fig. 4.

6 Modeling of SCFCs using ANN

In the previous section, SCFCs were determined using NSGA-II based on 125 experimental tests. In order to obtain SCFCs for non-experimented conditions, ANN models were taken into consideration. ANNs are widely used in modeling

Table 1 NSGA-II parameters

Parameter	Value
Population	100
Generation	100
Crossover	0.8
Mutation	0.2

Table 2 Cutting conditions of experimental work

Cutting condition	Range
Feed per tooth f_t (mm)	0.03, 0.05, 0.07, 0.09, 0.12
Cutting speed v_c (m/min)	64, 122, 166, 220, 256
DOC a_p (mm)	0.25, 0.5, 0.8, 1.1, 1.5

of machining processes such as turning, milling, and drilling [25, 26].

ANNs could present a robust method to simulate complex and unknown problems. Each of the parameters such as hidden layer number, training algorithm, the number of neurons in each layer, and the activation function of hidden layers can influence the results [27]. Back-propagation algorithm is a common algorithm for training and testing ANNs. In this study, the five feed forward back-propagation algorithms, i.e., Levenberg–Marquardt (LM), Bayesian regularization (BR), resilient propagation (RP), conjugate gradient Fletcher (CGF), and Broyden–Fletcher–Goldfarb (BFG), are used to train ANNs. Furthermore, various activation functions are used in hidden layers, namely logarithmic sigmoid function (Logsig) and the hyperbolic tangent sigmoid function (Tansig). In the output layer, the linear function (Purelin) is used. The cutting speed, feed per tooth, and DOC are input dataset parameters of the network. The output of the neural networks are desired SCFCs for the given cutting condition.

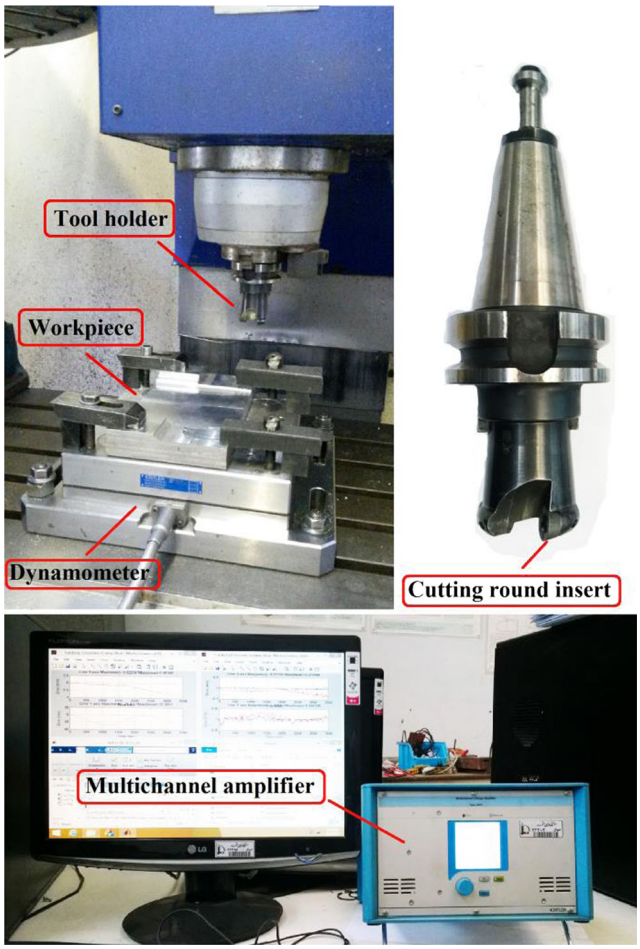

Fig. 4 Experimental setup for measuring the cutting force components and data acquisition

In order to increase the efficiency and accuracy of the predictions, each of SCFCs is modeled in a separate neural network (six ANN models). The neural network topology used in the present work is shown in Fig. 5. The input/output dataset was divided randomly into two groups, i.e., training dataset and test dataset. The training dataset consists of 75 % of input/output dataset, and the remaining 25 % is used as the test dataset [27].

Training and test output datasets of neural networks are SCFCs which have been determined by NSGA-II introduced in Sect. 5. The number of hidden layers, the number of neurons in each layer, the training algorithm, the activation function of hidden layers, and the output layer are investigated in a certain range using trial and error method. The main parameters' ranges of the neural network are shown in Table 3. Training and testing procedure of each neural network is implemented in MATLAB software. The multi-layer perceptron (MLP) type of ANN has been used for training and testing ANNs. Each of multi-layer ANNs consist of three inputs (cutting parameter) and one output (each of SCFCs). The two-layer perceptron back-propagation with the training epoch of 1000 is used in order to predict the SCFCs. A criterion to select the best network is the mean absolute percentage error of training ($MAPE_{tr}$) and testing ($MAPE_{ts}$) datasets which defines as follows:

$$MAPE_{tr}\&\ MAPE_{ts}\ \% = \frac{1}{N}\sum_{t=1}^{N}\left|\frac{D_{pre}-D_{exp}}{D_{exp}}\right| * 100 \qquad (10)$$

where N is the number of training or testing dataset, and D_{pre} and D_{exp} are the predicted and measured values, respectively. As reported in Table 4, six networks with the least mean absolute percentage error of training and testing were selected as the best networks to predict each SCFC. As seen in Table 4, the maximum mean absolute percentage error, which was considered for the training and testing of ANN models, is

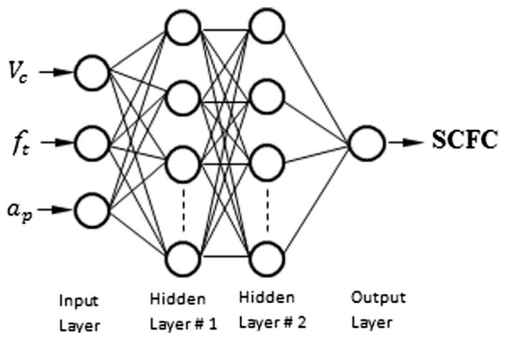

Fig. 5 Predictive SCFCs model topology

Table 3 Main parameters' range for neural network modeling

Parameter	Investigated range
Hidden layer	1 or 2 layer(s)
No. of each layer's neurons	1 to 30
Training algorithm	LM; BR; CGF; BFG; RP
Activation function	Tansig; Logsig

10.1 %. Therefore, the two-layer ANN is suitable for prediction of SCFCs. The training mean absolute percentage error ($MAPE_{tr}$) values of k_{tc} and k_{rc} are 1.7 and 4 %, respectively. Also, the testing mean absolute percentage error ($MAPE_{ts}$) values of k_{tc} and k_{rc} are 3.6 and 9.7 %, respectively. Therefore, the ANN results can be used as an acceptable database to develop the regression model for evaluating interactions of the cutting parameters on k_{tc} and k_{rc} value variation. In order to assess the training of designed ANNs, a number of experimental and ANN output datasets are evaluated. Figures 6 and 7 are compared the tangential and radial SCFCs of experimental and the ANN prediction results. As mentioned before, the training and test output datasets of ANNs are the SCFCs which have been determined by 125 experimental tests. It can be noted that the experimental and the predicted data are in appropriate accordance. Thus, the training of ANNs is accurately performed.

7 Results and discussion

In this section, face milling cutting forces are computed using the force model proposed in Sect. 3. The SCFCs of simulated cutting forces are obtained by NSGA-II and ANNs. The cutting parameter interaction on k_{tc} and k_{rc} variations are then investigated, and the results are thoroughly discussed.

7.1 Cutting force simulation

In order to validate the performance of NSGA-II and ANN in prediction of SCFCs, cutting forces of the face mill cutting process with round insert is simulated and compared to the

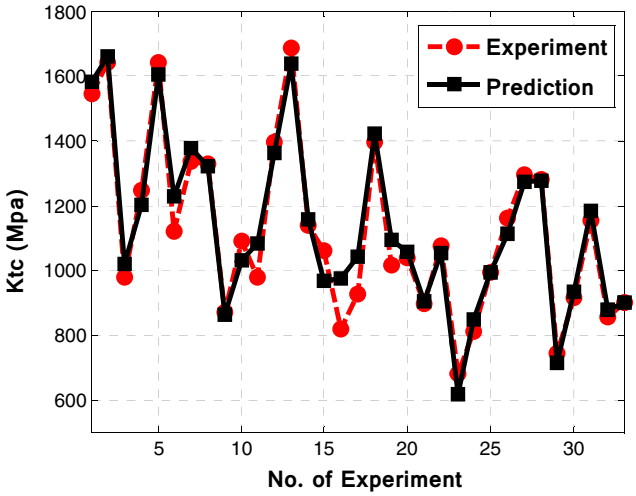

Fig. 6 Comparison of k_{tc} obtained from ANN and experimental data

experimental results. Figure 8 shows simulated and measured cutting forces for cutting speed v_c=220 m/min, feed per tooth f_t=0.05 mm, and DOC a_p=0.25 mm. This figure represents one of the 125 experiments in which SCFCs of the cutting force model are determined using NSGA-II. The excellent accordance between simulated and measured cutting forces confirms validness of NSGA-II. Therefore, the NSGA-II is an accurate way for identification of SCFCs of a mechanistic cutting force model. Figure 9 shows simulated and measured cutting forces for cutting speed v_c=144 m/min, feed per tooth f_t=0.07 mm, and DOC a_p=1.25 mm. It should be noted that SCFCs of the simulation are predicted using ANN models. The good agreement between the simulated and measured cutting forces proves the capability of ANN models to predict the SCFCs for non-experimented cutting conditions.

7.2 Cutting parameters interaction on k_{tc} and k_{rc} variations

In addition to the process prediction, ANN models can be effectively used for the evaluation of cutting parameter interaction. In the current research, the mathematical function developed by the ANN modeling is used for evaluating interactions of the cutting speed, feed per tooth, and DOC on k_{tc} and

Table 4 Specifications of the best networks which selected for each of SCFCs

SCFC	No. of first hidden layer's neurons	No. of second hidden layer's neurons	Training algorithm	Activation function of first hidden layer	Activation function of second hidden layer	$MAPE_{tr}$ (%)	$MAPE_{ts}$ (%)
K_{tc}	3	3	BR	Logsig	Tansig	1.7	3.6
K_{rc}	6	3	BR	Tansig	Logsig	4	9.7
K_{ac}	5	2	BR	Logsig	Logsig	9.19	10.1
K_{te}	8	22	BR	Logsig	Logsig	2.8	7.3
K_{re}	18	25	CGF	Tansig	Logsig	6.57	7.55
K_{ae}	27	24	LM	Tansig	Logsig	2.58	8.2

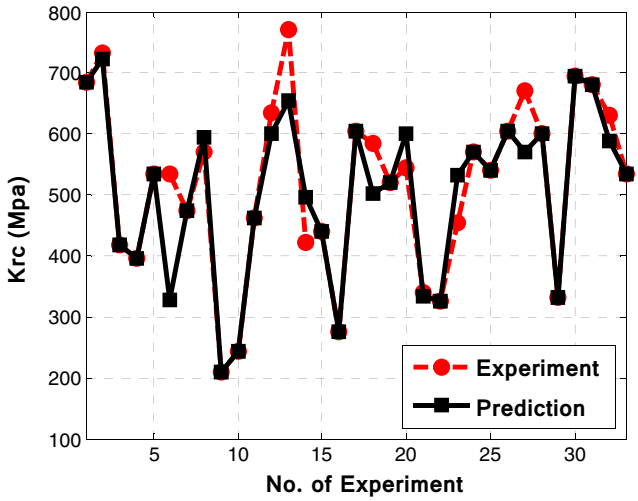

Fig. 7 Comparison of k_{rc} obtained from ANN and experimental data

k_{rc} values. 3D surfaces and their contours are proposed to comprehensively study the interactions.

7.2.1 Cutting speed and feed per tooth interaction

In Figs. 10 and 11, the cutting speed and feed per tooth interaction on k_{tc} and k_{rc} in constant DOC a_p=0.75 mm are shown, respectively.

It can be seen that by increasing feed per tooth and decreasing cutting speed, both of k_{tc} and k_{rc} are declined. The observed trend is in accordance with the size effect [28–30]. The following equation precisely expresses the size effect [29]:

$$K = B(t_c)^p \tag{11}$$

where K is SCFC, t_c is an uncut chip thickness, B and p are constants depending on tool geometry and materials. Based on the size effect, for small values of the uncut chip thickness, k_{tc} and k_{rc} are reduced by increasing feed per tooth.

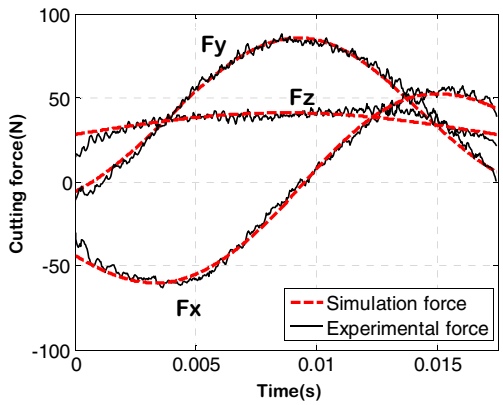

Fig. 8 Comparison of simulated and measured cutting forces; SCFCs of simulation are determined using NSGA-II

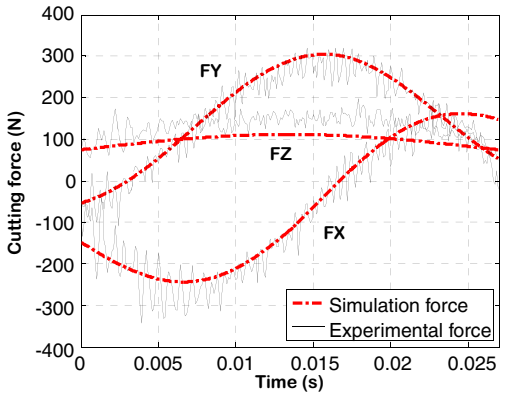

Fig. 9 Comparison of the simulated cutting forces obtained from ANN models with the measured cutting forces

7.2.2 Feed per tooth and DOC interaction

The interaction of feed per tooth and DOC which influences on k_{tc} and k_{rc} is illustrated in Figs. 12 and 13 for cutting speed v_c=100 m/min. According to Fig. 12, by increasing feed per tooth and DOC, the value of k_{tc} is reduced. The distinguished feature of round inserts is that the variation of the uncut chip

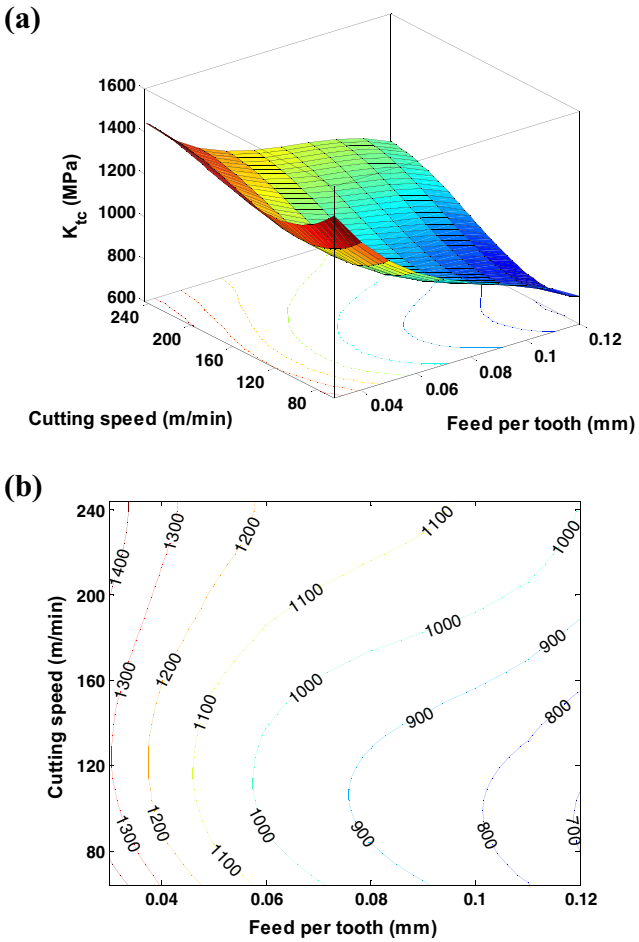

Fig. 10 Feed per tooth and cutting speed interaction on k_{tc} at DOC a_p= 0.75 mm

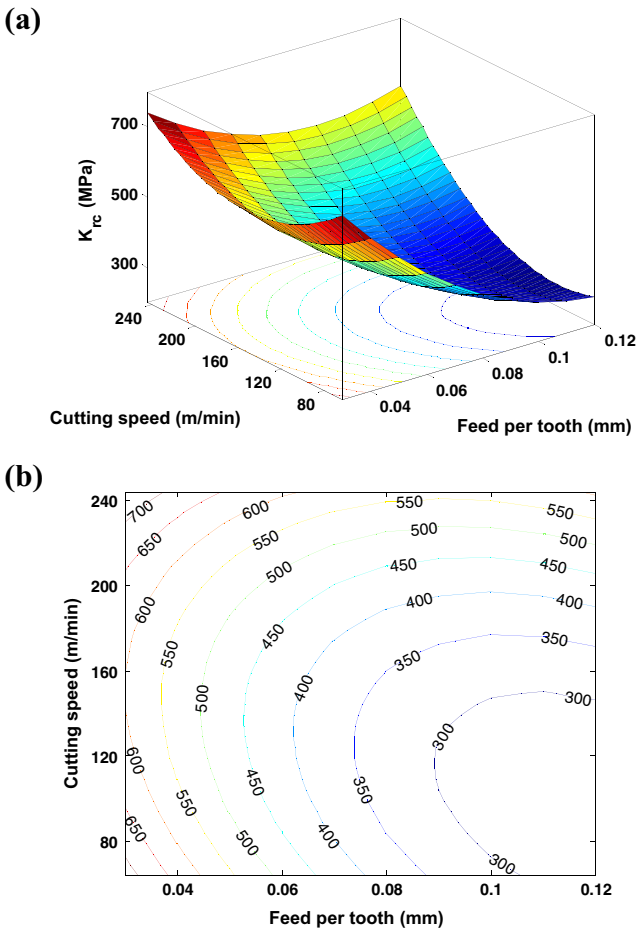

Fig. 11 Feed per tooth and cutting speed interaction on k_{rc} at DOC a_p= 0.75 mm

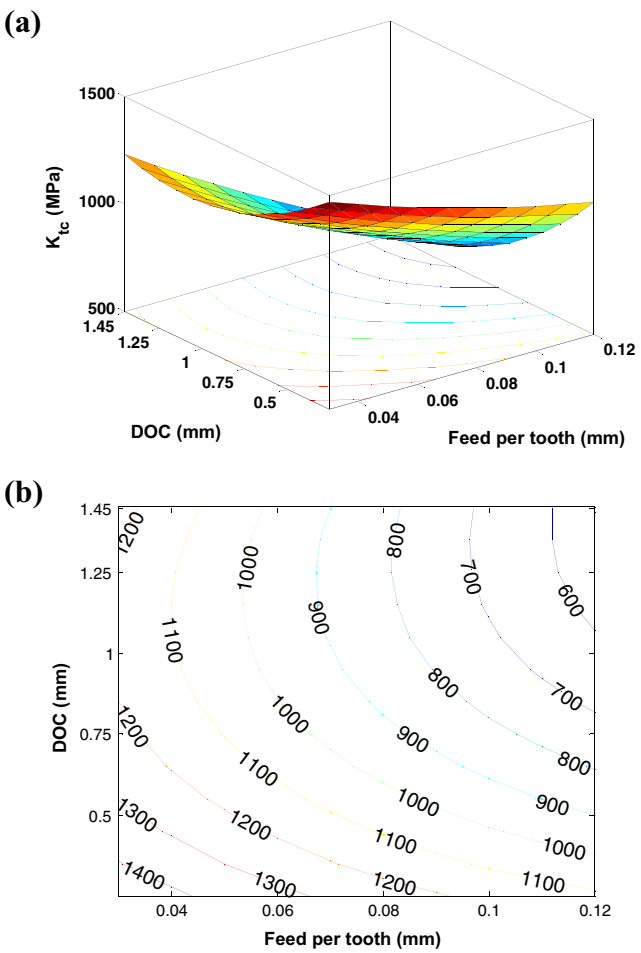

Fig. 12 Feed per tooth and DOC interaction on k_{tc} at cutting speed v_c= 100 m/min

thickness not only depends on the feed per tooth but also is determined by DOC. The chip thickness distribution along the round insert is illustrated in Fig. 14. As can be seen in Fig. 14, by increasing DOC, chip thickness gradually increases.

For a certain DOC, the equivalent chip thickness is defined as follows [31]:

$$h_{eq} = \frac{\sum_{j=1}^{P} h_j}{P} \tag{12}$$

where h_j is the chip thickness of jth discrete element and P is the total number of elements on the cutting edge.

According to Fig. 14 and Eq. 12, by increasing DOC and feed per tooth simultaneously, chip thickness is increased and k_{tc} is reduced. It should be noted that the size effect is intense for small values of the uncut chip thickness. On the other hand, for higher values of DOC, a_p> 0.85 mm, and the desired range of feed per tooth, the k_{tc} value is almost constant (see Fig. 12).

The parameters which influence variations of k_{rc} are chip thickness and cutting edge geometry. Increase in chip thickness leads to decrease in k_{rc}. On the other hand, for round insert geometry, increase in DOC results in reduction of lead angle (γ_l). Consequently, the ratios of radial cutting force to axial cutting force $\frac{F_R}{F_A}$, and accordingly, the k_{rc} are increased.

At low DOCs, the dominant mechanism which leads to decreasing k_{rc} is size effect. In other words, for low values of DOCs by increasing feed per tooth and DOC concurrently, k_{rc} is declined, see Fig. 13. The ratios of radial cutting force to axial cutting force $\frac{F_R}{F_A}$ are computed along line AB (in triangle points) of Fig. 13b and are depicted as a black line in Fig. 15. At low DOCs (a_p< 0.85 mm), the $\frac{F_R}{F_A}$ ratio is reduced by increasing the feed per tooth and DOC. This trend indicates at low DOCs, the size effect is the dominant mechanism which results in reduction of k_{rc} and consequently radial cutting force component (F_R).

At higher DOCs, the trend of $\frac{F_R}{F_A}$ ratio variation is reversed. In other words, by increasing the feed per tooth and DOC simultaneously, the ratio of $\frac{F_R}{F_A}$ is increasing. Thus, for higher values of feeds per tooth (f_t>0.08 mm) and DOCs (a_p> 0.85 mm), the k_{rc} is grown.

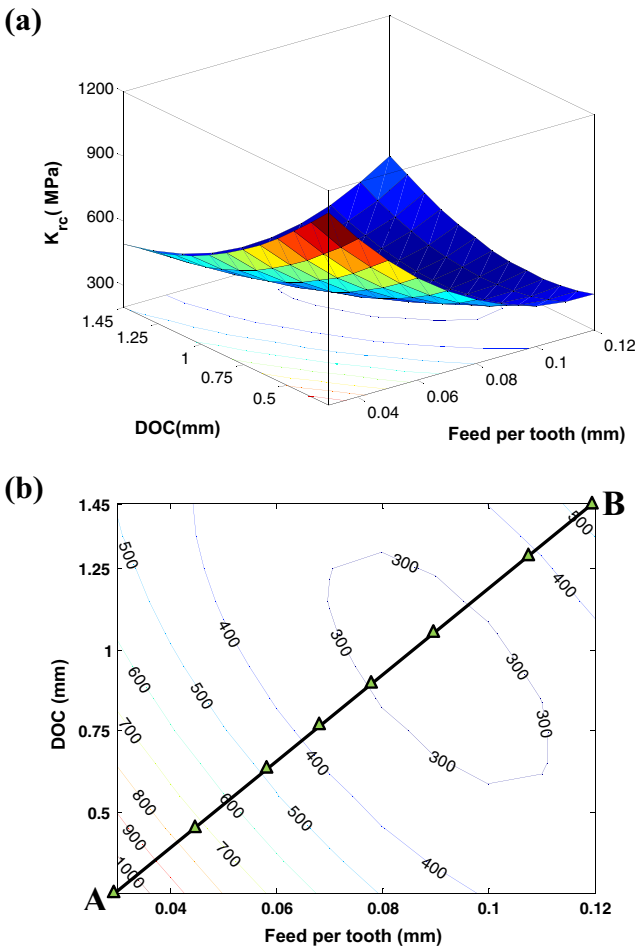

Fig. 13 Feed per tooth and DOC interaction on k_{rc} at cutting speed of v_c= 100 m/min

7.2.3 Cutting speed and DOC interaction

The interaction of cutting speed and DOC on k_{tc} at feed per tooth f_t=0.1 mm is shown in Fig. 16. By increasing DOC and decreasing the cutting speed concurrently, the value of k_{tc} is reduced.

The variations of k_{rc} is decreasing for low cutting speeds and DOCs. But, for higher values of cutting speed and DOC, i.e., v_c>140 m/min and a_p>0.8 mm, the variations of k_{rc} is increased (see Fig. 17). Figure 15 also illustrates the variation

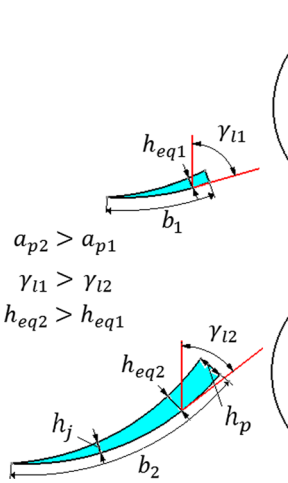

Fig. 14 Variation of lead angle (γ_l) and equivalent chip thickness (h_{eq}) along the cutting edge by increasing DOC

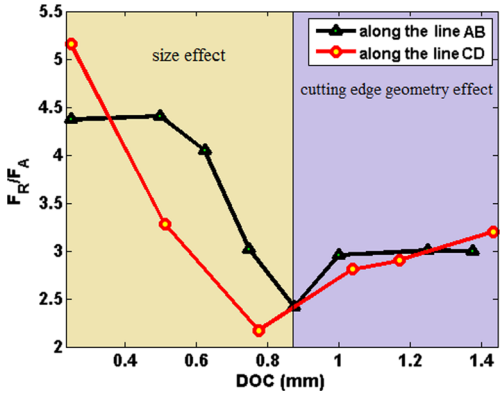

Fig. 15 Ratio of radial cutting force to axial cutting force $\frac{F_R}{F_A}$ versus cutting DOC. *Triangles* correspond to line AB in Fig. 13b, and *circles* correspond to line DC in Fig. 17b

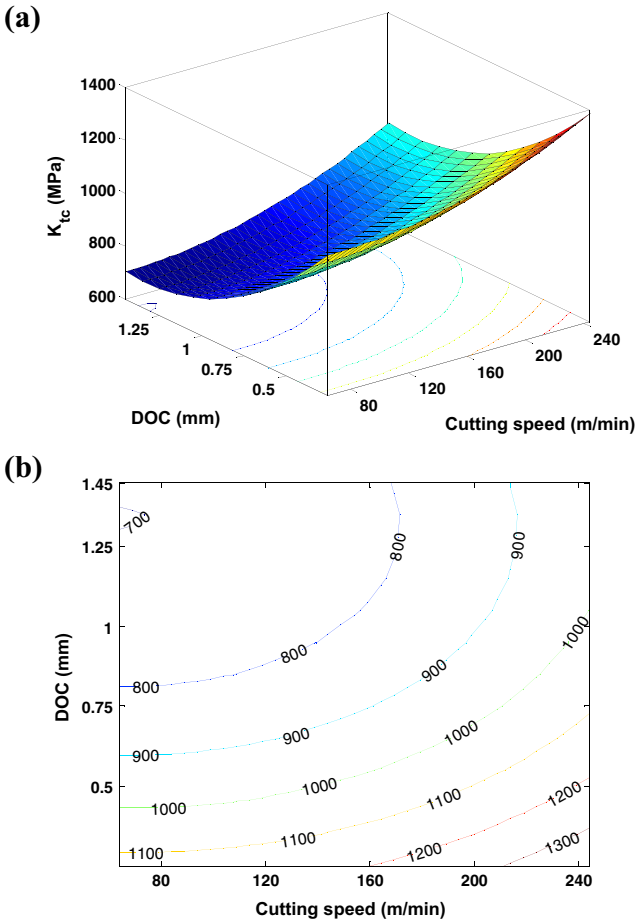

Fig. 16 Cutting speed and DOC interaction on k_{tc} at feed per tooth f_t= 0.1 mm

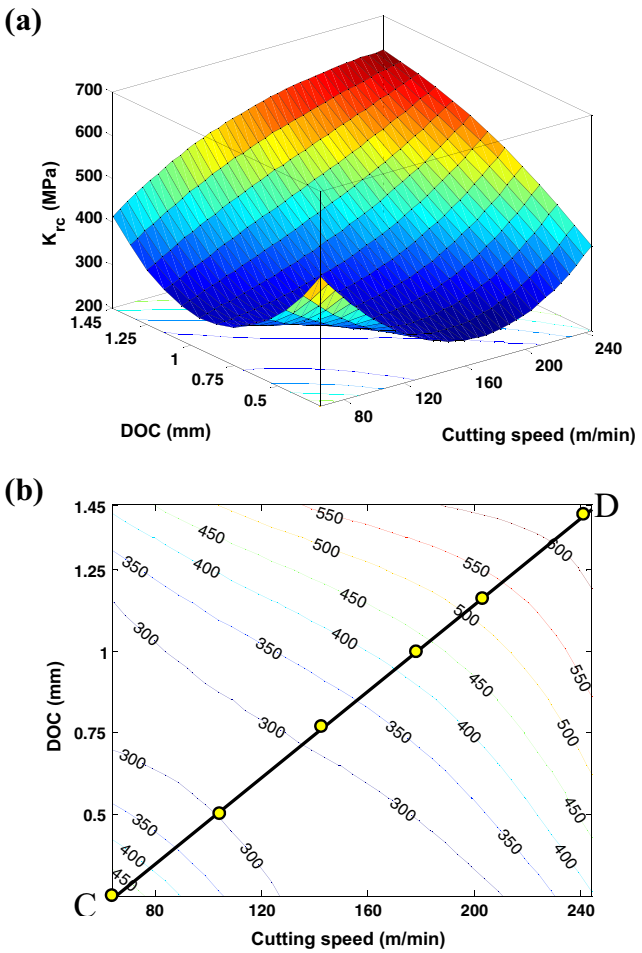

Fig. 17 Cutting speed and DOC interaction on k_{rc} at feed per tooth f_t= 0.1 mm

of $\frac{F_R}{F_A}$ ratios by red line for the circle points along line CD which are depicted in Fig. 17b. With respect to cutting speed and DOC interaction, it can be noted that for small values of DOC the dominant mechanism is the size effect which leads to decreasing k_{rc}, while for higher values of DOC the ratio of $\frac{F_R}{F_A}$ is increasing and the dominant mechanism is the cutting edge geometry which results in reduction of k_{rc}.

8 Conclusions

Due to complex geometry of the round insert, the pronounced effects of cutting edge entrance and exit zones on the cutting forces, the instantaneous cutting forces during engagement must be measured and used to determine the SCFCs. In the current work, the proposed mechanistic cutting force model is considered as a three-objective optimization problem. One hundred twenty-five experiments are conducted at desired values of cutting conditions which are repeated three times in order to assure the validity of experimental data. SCFCs for each experimental result are obtained by NSGA-II.

The prediction of SCFCs for non-experimented cutting conditions is performed by the ANN models. Training and testing output dataset of each six neural networks are SCFCs obtained by NSGA-II. Training dataset consists of 75 % of input/output dataset, and the remaining 25 % is used as the test dataset. In this research, the five feed forward back propagation algorithms, namely LM, BR, RP, CGF, and BFG, are used to train ANNs. The multi-layer perceptron back-propagation algorithm (BPA) with the training epoch of 1000 is used in order to predict the SCFCs. Each of multi-layer networks consists of three inputs (cutting parameter) and one output (each of SCFCs). In various tries, the mean absolute percentage error of ANN models of SCFCs were between 1.7 and 9.19 % for training ($MAPE_{tr}$) and between 3.6 and 10.1 % for testing ($MAPE_{ts}$) which are acceptable (see Table 4).

The $MAPE_{tr}$ of k_{tc} and k_{rc} are 1.7 and 4 % respectively. In addition, the $MAPE_{ts}$ values are 3.6 and 9.7 % respectively. Therefore, the ANN results are used as an acceptable database to develop the regression model for evaluating interactions of the cutting parameters on k_{tc} and k_{rc} variations.

The accuracy of the optimization method and ANN models is validated by simulated and experimental cutting forces. In addition, it is demonstrated that the data obtained from multi-objective optimization method can be used as training and testing output dataset for ANN modeling.

Moreover, the cutting parameters interaction i.e., cutting speed, feed per tooth, and DOC interactions on k_{tc} and k_{rc} are thoroughly investigated. The cutting edge geometry of round insert plays an important role in k_{tc} and k_{rc} variations. By increasing DOC for a round insert, chip thickness increases and k_{tc} and k_{rc} values reduces according to the size effect. Furthermore, increasing DOC results in higher ratios of radial component to axial component of the cutting force $\frac{F_R}{F_A}$ and accordingly increasing k_{rc}. At low DOCs, the size effect is the dominant mechanism affecting k_{tc} and k_{rc} reductions. However, at high DOCs, ratio of radial force to axial force $\frac{F_R}{F_A}$ is increased and k_{rc} is grown.

The results developed in this research can be used by machining experts in order to estimate the efficient cutting parameters, i.e., cutting speed, feed per tooth, and depth of cut for round insert prior to machining operations. Moreover, selection of the proper depth of cuts which lead to decreasing the ratio of radial cutting force to axial cutting force, could be of great practical significance. By decreasing $\frac{F_R}{F_A}$, the distribution of cutting forces in the axial direction has been increased, thus vibration generated due to long tool overhangs is reduced and workpiece surface quality is improved.

References

1. Lee W-Y, Kim K-W, Sin H-C (2002) Design and analysis of a milling cutter with the improved dynamic characteristics. Int J Mach Tool Manuf 42(8):961–967
2. Gradišek J, Kalveram M, Weinert K (2004) Mechanistic identification of specific force coefficients for a general end mill. Int J Mach Tool Manuf 44(4):401–414
3. Kaymakci M, Kilic Z, Altintas Y (2012) Unified cutting force model for turning, boring, drilling and milling operations. Int J Mach Tool Manuf 54:34–45
4. Van Luttervelt C, Childs T, Jawahir I, Klocke F, Venuvinod P, Altintas Y, Armarego E, Dornfeld D, Grabec I, Leopold J (1998) Present situation and future trends in modelling of machining operations progress report of the CIRP Working Group 'Modelling of Machining Operations'. CIRP Ann Manuf Technol 47(2):587–626
5. Barge M, Hamdi H, Rech J, Bergheau J-M (2005) Numerical modelling of orthogonal cutting: influence of numerical parameters. J Mater Process Technol 164:1148–1153
6. Jin X, Altintas Y (2012) Prediction of micro-milling forces with finite element method. J Mater Process Technol 212(3):542–552
7. Ehmann K, Kapoor S, DeVor R, Lazoglu I (1997) Machining process modeling: a review. J Manuf Sci Eng 119(4B):655–663
8. Altintas Y (2012) Manufacturing automation: metal cutting mechanics, machine tool vibrations, and CNC design. Cambridge University Press, Cambridge
9. Gao G, Wu B, Zhang D, Luo M (2013) Mechanistic identification of cutting force coefficients in bull-nose milling process. Chin J Aeronaut 26(3):823–830
10. Imani B, Sadeghi M, Elbestawi M (1998) An improved process simulation system for ball-end milling of sculptured surfaces. Int J Mach Tool Manuf 38(9):1089–1107
11. Feng H-Y, Menq C-H (1994) The prediction of cutting forces in the ball-end milling process—I. Model formulation and model building procedure. Int J Mach Tool Manuf 34(5):697–710
12. Budak E, Altintas Y, Armarego E (1996) Prediction of milling force coefficients from orthogonal cutting data. J Manuf Sci Eng 118(2): 216–224
13. Gonzalo O, Beristain J, Jauregi H, Sanz C (2010) A method for the identification of the specific force coefficients for mechanistic milling simulation. Int J Mach Tool Manuf 50(9):765–774
14. Lamikiz A, López de Lacalle L, Sánchez J, Bravo U (2005) Calculation of the specific cutting coefficients and geometrical aspects in sculptured surface machining. Mach Sci Technol 9(3):411–436
15. Azeem A, Feng H-Y, Wang L (2004) Simplified and efficient calibration of a mechanistic cutting force model for ball-end milling. Int J Mach Tool Manuf 44(2):291–298
16. Wang M, Gao L, Zheng Y (2014) An examination of the fundamental mechanics of cutting force coefficients. Int J Mach Tool Manuf 78:1–7
17. Baro PK, Joshi SS, Kapoor S (2005) Modeling of cutting forces in a face-milling operation with self-propelled round insert milling cutter. Int J Mach Tool Manuf 45(7):831–839
18. Pérez RV (2005) Wear mechanisms of WC inserts in face milling of gamma titanium aluminides. Wear 259(7):1160–1167
19. Konak A, Coit DW, Smith AE (2006) Multi-objective optimization using genetic algorithms: a tutorial. Reliab Eng Syst Saf 91(9):992–1007
20. Marler RT, Arora JS (2004) Survey of multi-objective optimization methods for engineering. Struct Multidiscip Optim 26(6):369–395
21. Wang Q, Liu F, Wang X (2014) Multi-objective optimization of machining parameters considering energy consumption. Int J Adv Manuf Technol 71(5–8):1133–1142
22. Yang S, Natarajan U (2010) Multi-objective optimization of cutting parameters in turning process using differential evolution and non-dominated sorting genetic algorithm-II approaches. Int J Adv Manuf Technol 49(5–8):773–784
23. Yusup N, Zain AM, Hashim SZM (2012) Evolutionary techniques in optimizing machining parameters: review and recent applications (2007–2011). Expert Syst Appl 39(10):9909–9927
24. Yusoff Y, Ngadiman MS, Zain AM (2011) Overview of NSGA-II for optimizing machining process parameters. Procedia Eng 15: 3978–3983
25. El-Mounayri H, Briceno JF, Gadallah M (2010) A new artificial neural network approach to modeling ball-end milling. Int J Adv Manuf Technol 47(5–8):527–534
26. Karabulut Ş (2015) Optimization of surface roughness and cutting force during AA7039/Al 2 O 3 metal matrix composites milling using neural networks and Taguchi method. Measurement 66: 139–149
27. Aykut Ş, Gölcü M, Semiz S, Ergür H (2007) Modeling of cutting forces as function of cutting parameters for face milling of satellite 6 using an artificial neural network. J Mater Process Technol 190(1): 199–203
28. Balogun VA, Mativenga PT (2014) Impact of un-deformed chip thickness on specific energy in mechanical machining processes. J Clean Prod 69:260–268
29. Ko JH, Yun W-S, Cho D-W, Ehmann KF (2002) Development of a virtual machining system, part 1: approximation of the size effect for cutting force prediction. Int J Mach Tool Manuf 42(15):1595–1605
30. Melkote S, Endres W (1998) The importance of including size effect when modeling slot milling. J Manuf Sci Eng 120(1):68–75
31. Bouzakis K-D, Aichouh P, Efstathiou K (2003) Determination of the chip geometry, cutting force and roughness in free form surfaces finishing milling, with ball end tools. Int J Mach Tool Manuf 43(5): 499–514